Supplementary Material for

Correlation between Si-Al disorder and hydrogen-bonding distance variation in ussingite (Na$_2$AlSi$_3$O$_8$OH) revealed by one- and two-dimensional multi-nuclear NMR and first-principles calculation

Xianyu Xue* and Masami Kanzaki

Institute for Planetary Materials, Okayama University, Yamada 827, Misasa, Tottori Japan
* Corresponding author; E-mail: xianyu@misasa.okayama-u.ac.jp

Content:

Raman spectroscopy

References cited

Supplementary Tables:

Supplementary figures:

Raman spectroscopy

Unpolarized Raman spectra in the 0~4500 cm^{-1} region were acquired at selected spots on large pieces of ussingite for both samples by 180° backscattering geometry. It was found that the OH stretching vibration region could not be observed well at an excitation wavelength of 488 nm due to broad fluorescence band. Measurements were thus made with a 532 nm solid-state laser at 100 mW output. A very strong fluorescent doublet from the samples was found to occur at 810 nm. Ghosts of the doublet also appear in the frequency range of measurement, but was removed by inserting a 750 nm short-pass filter.

For Raman measurement, the laser beam was focused onto the sample with a 20× objective lens. The scattered light from the sample was focused on a pinhole (diameter: 200 μm), collimated, and then passed through a 750 nm short-pass filter and a Raman long-pass filter (Semrock Inc., RazorEdge filter), before entering an imaging monochromator with a focal length of 500 mm and a grating of 300 gr/mm, and detected by a CCD detector cooled with liquid nitrogen (Teledyne Princeton Instruments, PyLoN 400BR eXcelon). The laser wavelength and Raman shift were calibrated using the emission lines of Ne lamp with an accuracy better than 5 cm^{-1}. The exposure time was typically 10 s, and the spectra were stacked 6 times.

Raman spectra in the 0~4500 cm^{-1} region obtained at several spots of both ussingite samples were found to be similar, with variations in relative intensities that largely reflect different orientations. A typical spectrum for sample 2 is shown in Figure 2s. The spectra are overall similar to those in the RRUFF database for ussingite from Ilimaussaq, Greenland (Lafuente et al., 2015). Within the high-frequency region, broad bands with at least three maxima (1800~1870, 2390, 2620 cm^{-1}) can be recognized. Broad bands between 800 and 3000 cm^{-1} with several peak maxima (and minima) have also been reported for infrared absorption spectra of ussingite from Ilimaussaq, Greenland (Johnson and Rossman, 2004). Very broad bands spanning a wide frequency range to well below 2000 cm^{-1} with several maxima are typical of strongly hydrogen-bonded OH, and the multiple maxima are generally regarded to result from Fermi resonance with other vibrational modes, such as bending vibrations.

References Cited

Amoureux, J.-P., and Fernandez, C. (1998) Triple, quintuple and higher order multiple quantum MAS NMR of quadrupolar nuclei Solid State Nuclear Magnetic Resonance, 10(4), 211-223.

Amoureux, J.P., Delevoye, L., Steuernagel, S., Gan, Z., Ganapathy, S., and Montagne, L. (2005) Increasing the sensitivity of 2D high-resolution NMR methods applied to quadrupolar nuclei. Journal of Magnetic Resonance, 172(2), 268-278.

Gan, Z.H., and Kwak, H.T. (2004) Enhancing MQMAS sensitivity using signals from multiple coherence transfer pathways. Journal of Magnetic Resonance, 168(2), 346-351.

Hohwy, M., Jakobsen, H.J., Eden, M., Levitt, M.H., and Nielsen, N.C. (1998) Broadband dipolar recoupling in the nuclear magnetic resonance of rotating solids: A compensated C7 pulse sequence. Journal of Chemical Physics, 108(7), 2686-2694.

Ishii, Y., and Tycko, R. (2000) Sensitivity enhancement in solid state ^{15}N NMR by indirect detection with high-speed magic angle spinning. Journal of Magnetic Resonance, 142(1), 199-204.

Johnson, E.A., and Rossman, G.R. (2004) An infrared and ^{1}H MAS NMR investigation of strong hydrogen bonding in ussingite, $Na_2AlSi_3O_8(OH)$. Physics and Chemistry of Minerals, 31(2), 115-121.

Lafuente, B., Downs, R.T., Yang, H., and Stone, N. (2015) The power of databases: the RRUFF project. In T. Armbruster, and R.M. Danisi, Eds. Highlights in Mineralogical Crystallography, p. 1-30. W. De Gruyter, Berlin, Germany.

Torchia, D.A. (1978) Measurement of proton-enhanced C-13 T1 values by a method which suppresses artifacts. Journal of Magnetic Resonance, 30(3), 613-616.

Table 1s. Acquisition and processing parameters for NMR spectra reported in figures and tables:

Fig. 2a. ^{29}Si MAS NMR

Sample	Sample 1
Pulse sequence	Single pulse with decoupling
Resonance frequency (MHz)	79.487
Spinning rate (kHz)	20
Spectral width (kHz)	50
Pulse length (µs)	1.8 (45° flip angle)
Recycle delay (s)	4500
Acquisition time (s)	0.05
Number of scans	200
Decoupling	Swept-frequency-TPPM at a RF field of ~90 kHz
Line broadening	None

Fig. 2b & Table 2. ^{1}H-^{29}Si CP MAS NMR

Sample	Sample 1	Sample 2
Pulse sequence	CP MAS	CP MAS
Spinning rate (kHz)	10	10
Spectral width (kHz)	50	50
Recycle delay (s)	150	60
Contact time (ms)	12 & 20	12 & 20
CP condition	MAS-modified Hartman-Hahn condition (+1 spinning sideband for ^{1}H), with an RF field of ~32 kHz for ^{29}Si & ramped power (90-100%) for ^{1}H	
Acquisition time (s)	0.05	0.05
Number of scans	1000	3200 & 4000
Decoupling	Swept-frequency-TPPM at a RF field of ~90 kHz	
Line broadening	None	None

Fig. 3 and Table 3. ^{1}H MAS NMR

	Sample 1	Sample 2
Pulse sequence	DEPTH2	DEPTH2
Resonance frequency (MHz)	400.13	400.13
Spinning rate (kHz)	20 & 24	20 & 24

Spectral width (kHz)	200	200
Recycle delay (s)	400	300 & 150
Acquisition time (s)	0.02	0.02
Number of scans	16	128 & 64
Line broadening	None	None

Fig. 4a. 2D ^{1}H DQ MAS NMR

Sample	Sample 1
Pulse sequence	POST-C7
Spinning rate (kHz)	14.705
Spectral width (F2, F1) (kHz)	14.705, 14.705
Recycle delay (s)	100
DQ excitation, reconversion period (μs)	408, 408
z-filter delay (μs)	20
Acquisition time (s)	0.02
Number of scans	8
Number of t_1 increment	112
Quadrature detection	States-TPPI
Line broadening	None

Fig. 5a. 2D ^{1}H-^{29}Si HETCOR

Sample	Sample 1
Pulse sequence	^{1}H$\rightarrow$^{29}Si$\rightarrow$^{1}H double CP
Spinning rate (kHz)	24
Spectral width (F2, F1) (kHz)	24,12
Recycle delay (s)	100
Contact time (1st , 2nd CP) (ms)	8, 8
CP condition	MAS-modified Hartman-Hahn condition (+1 spinning sideband for ^{1}H), with RF field of ~32 kHz for ^{29}Si & ramped power (100 to 90% for the first CP period, and 90 to 100% for the second CP period) for ^{1}H
Rotary resonance recoupling period t_d (ms)	4
^{1}H RF field during t_d (kHz)	24

Acquisition time (s)	0.02
Number of scans	8
Number of t_1 increment	256
Quadrature detection	States-TPPI
Decoupling	None
Line broadening	None

Fig. 6. ^{27}Al MAS NMR

Sample	Sample 1
Pulse sequence	Single pulse
Resonance frequency (MHz)	104.261
Spinning rate (kHz)	20
Spectral width (kHz)	1875
Pulse length (μs)	0.3 (selective 30˚ flip angle for central transition)
Recycle delay (s)	2
Acquisition time (s)	0.01
Number of scans	18400
Decoupling	None
Line broadening	None
Linear prediction	backward for 22 complex point
Baseline correction	Spline

Fig. 7. ^{27}Al SPAM-3QMAS NMR

Sample	Sample 1
Pulse sequence	SPAM-3QMAS
Resonance frequency (MHz)	104.267
Spinning rate (kHz)	20
Spectral width (F2, F1) (kHz)	40, 20
Recycle delay (s)	26
Pulse length (p1, p2, p3) (μs)	3.4, 1.04, 10 (90˚ pulse)
RF field for p1& p2 (kHz)	137
Acquisition time (s)	0.02
Number of scans	48
Number of t_1 increment	128
Quadrature detection	Echo-Antiecho

Decoupling	None
Line broadening	None
F1 chemical shift convention	Universal scaling convention of Amouroux and Fernandez (1998)

Fig. 8a. ^{23}Na SPAM-3QMAS NMR

Sample	Sample 1
Pulse sequence	SPAM-3QMAS
Resonance frequency (MHz)	105.840
Spinning rate (kHz)	20
Spectral width (F2, F1) (kHz)	40, 20
Recycle delay (s)	30
Pulse length (p1, p2, p3) (µs)	4.8, 1.5, 10 µs (90˚ pulse)
RF field for p1 & p2 (kHz)	139
Acquisition time (s)	0.014
Number of scans	72
Number of t_1 increment	80
Quadrature detection	Echo-Antiecho
Decoupling	none
Line broadening (F2, F1) (Hz)	200, None
F1 chemical shift convention	Universal scaling convention of Amouroux and Fernandez (1998)

Fig. 8b. ^{23}Na MAS NMR

Sample	Sample 1
Pulse sequence	Single pulse
Resonance frequency (MHz)	105.840
Spinning rate (kHz)	20
Spectral width (kHz)	1875
Pulse length (µs)	0.4 (selective 30˚ flip angle for central transition)
Recycle delay (s)	2
Acquisition time (s)	0.02
Number of scans	20000
Decoupling	None
Line broadening	None
Linear prediction	Backward for 22 complex point

Table 2s. ^{29}Si, ^{1}H, ^{27}Al and ^{23}Na spin-lattice relaxation time contant (T_1) of ussingite

peak (ppm)	^{29}Si T_1 (s)[a]	
	sample 1 @10kHz	
-84.1	8215	
-87.9	7631	
-96.5	11751	

peak (ppm)	^{1}H T_1 (s)[b]	
	sample 1 @20kHz	sample 2 @20kHz
15.5	51	37
13.8	44	28
11.1	81	45

peak (ppm)	^{27}Al T_1 (s)[c]	
	sample 1 @20kHz	sample 2 @20kHz
54	8.7	6.0

peak	^{23}Na T_1 (s) [c]	
	sample 1 @20kHz	sample 2 @20kHz
-26	9.6	9.0

[a] Determined by CP inversion recovery (Touchia method);

[b] Determined by saturation recovery using DEPTH2 for detection;

[c] Determined by saturation recovery.

Table 3s. Simulation result for ^{1}H-^{29}Si CP MAS NMR spectrum obtained at a spinning rate of 10 kHz and contact time of 20 ms for sample 1 (shown in Fig. 4s)

Peak label	NNN	δ_i^{Si}(ppm)	FWHM (Hz)	xG/(1-x)L	Integral%	Integral% (Q^3 only)	Integral% (Q^3 only)
1	Q^3(3Al)	-80.96	116.53	1.00	1.57	2.08	2.08
2		-83.04	83.81	1.00	0.53	0.70	
3		-83.09	64.31	1.00	0.78	1.03	
4		-83.54	39.91	0.85	5.24	6.94	
5	Q^3(1Si,2Al)	-84.07	54.40	1.00	19.43	25.74	49.08
6		-84.61	42.62	0.83	6.93	9.18	
7		-84.95	72.42	1.00	2.53	3.35	
8		-85.85	97.61	1.00	1.62	2.14	
9		-87.94	27.54	0.45	34.41	45.57	
10	Q^3(2Si,1Al)	-88.57	32.95	0.86	0.65	0.86	47.53
11		-89.21	43.23	1.00	0.84	1.11	
12	Q^3(3Si)	-91.60	41.85	1.00	0.99	1.31	1.31
13		-95.88	25.43	1.00	0.46		
14		-96.24	25.34	1.00	6.64		
15	Q^4(3Si,1Al)	-96.65	37.64	0.85	11.37		
16		-96.94	91.73	1.00	3.67		
17		-98.67	141.55	1.00	2.36		
Sum					100.00		
Sum(Q^3)					75.51	100.00	100.00

δ_i^{Si}: ^{29}Si isotropic chemical shift; FWHM: Full width at half maximum;

xG/(1-x)L: Gaussian fraction in pseudo-Voigt function

Table 4s. Simulation result for ^1H MAS NMR spectrum obtained at a spinning rate of 24 kHz for sample 1 (shown in Fig. 5s)

Peak label	Group	δ_i^H(ppm)	FWHM (Hz)	xG/(1-x)L	Integral (%)	Integral (%)
1	15~16 ppm	15.81	72.39	1.00	1.79	9.57
2		15.56	79.10	1.00	1.72	
3		15.49	87.67	0.67	1.87	
4		15.16	121.01	0.00	4.18	
5	13~14 ppm	13.85	165.16	0.72	80.86	87.55
6		13.35	152.40	0.00	6.68	
7	11 ppm	11.08	149.64	0.57	2.89	2.89
Sum					100.00	100.00

δ_i^H: ^1H isotropic chemical shift; FWHM: Full width at half maximum;

xG/(1-x)L: Gaussian fraction in pseudo-Voigt function

Figure 1s. Photos for the two ussingite samples studied. (Left) Sample 1 (purchased from Mineral Street) from Alluaiv Mt, Lovozero, Kola Peninsula, Russia. (Right): Sample 2 (purchased from eBay) described as from Greenland.
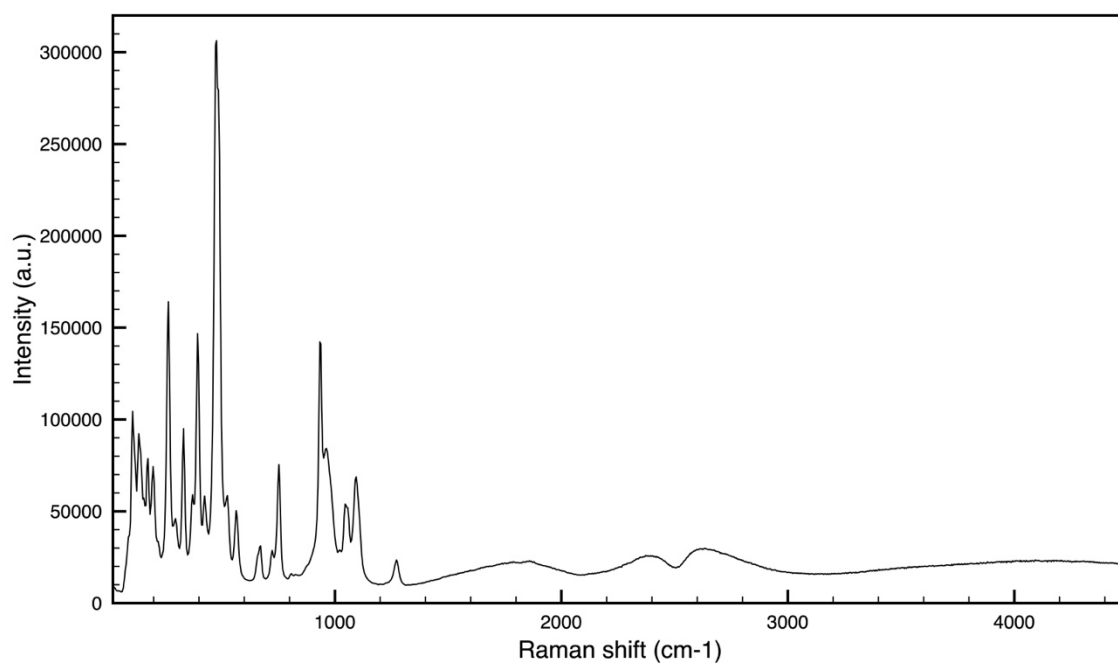
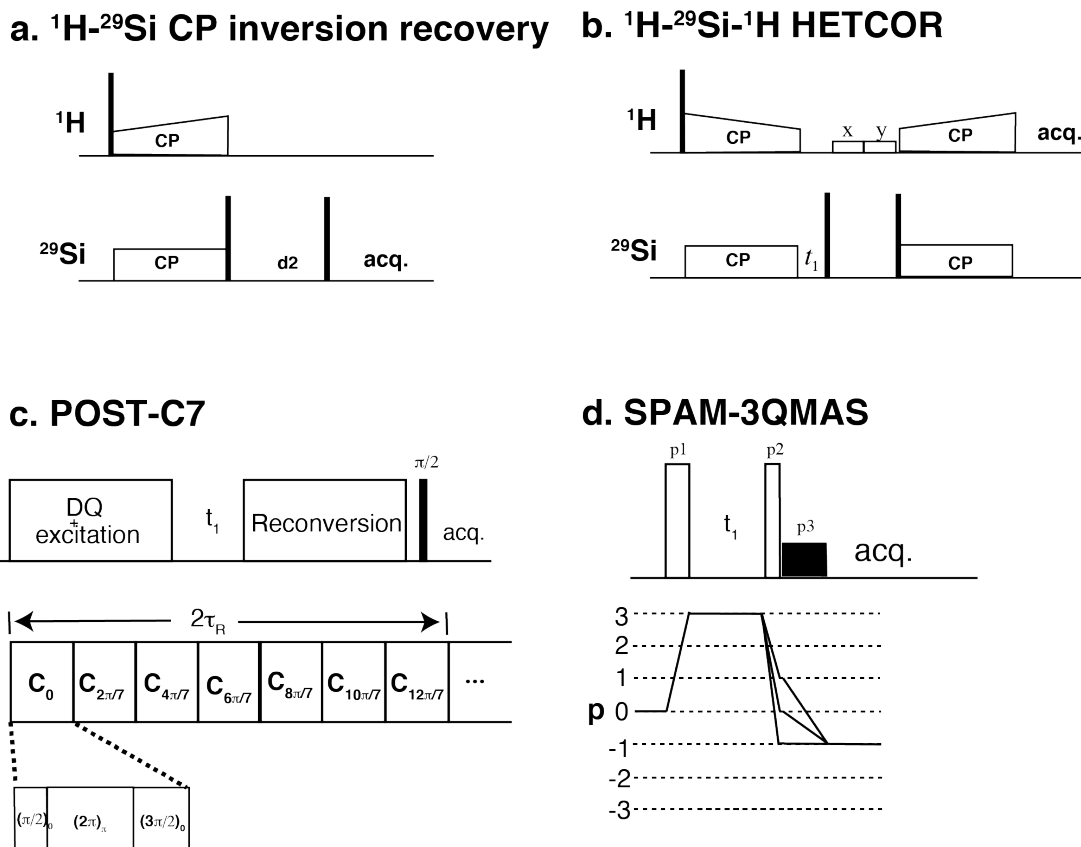Figure 2s. Unpolarized Raman spectrum for ussingite sample 2.

a. ^{1}H-^{29}Si CP inversion recovery
b. ^{1}H-^{29}Si-^{1}H HETCOR
c. POST-C7
d. SPAM-3QMAS

Figure 3s. Pulse sequences used. **(a)** CP inversion recovery experiment (Torchia, 1978) for the determination of ^{29}Si T_1. **(b)** 2D ^{1}H-^{29}Si HETCOR experiment with the ^{1}H→^{29}Si→^{1}H double CP MAS NMR technique (Ishii and Tycko, 2000). During rotary resonance recoupling period (t_d), a pair of long pulses with orthogonal phases (X and Y) and RF field satisfying the rotary resonance condition (equal to the one rotation frequency) was applied to ^{1}H to eliminate residual ^{1}H polarization. **(c)** ^{1}H DQ MAS NMR experiment with the POST-C7 pulse scheme (Hohwy et al., 1998) for DQ excitation/reconversion. The DQ excitation/reconversion period consists of 7 concatenated POST-C7 elements in two rotor periods (τ_R) with each element containing three pulses and the overall phase of the POST-C7 elements being incremented successively by $2\pi/7$. **(d)** 2D 3Q MAS NMR experiment using the SPAM (soft-pulse added mixing)-3QMAS pulse scheme (Amoureux et al., 2005; Gan and Kwak, 2004). The pulse sequence consists of two hard pulses for 3Q excitation and 3Q→0Q, ±1Q reconversion, followed by a soft $\pi/2$ pulse for detection, with echo and anti-echo signals detected alternatively for each t_1 increment. Only one of the two pathways (echo for ^{27}Al (I = 5/2), anti-echo for ^{23}Na (I = 3/2)) is shown.
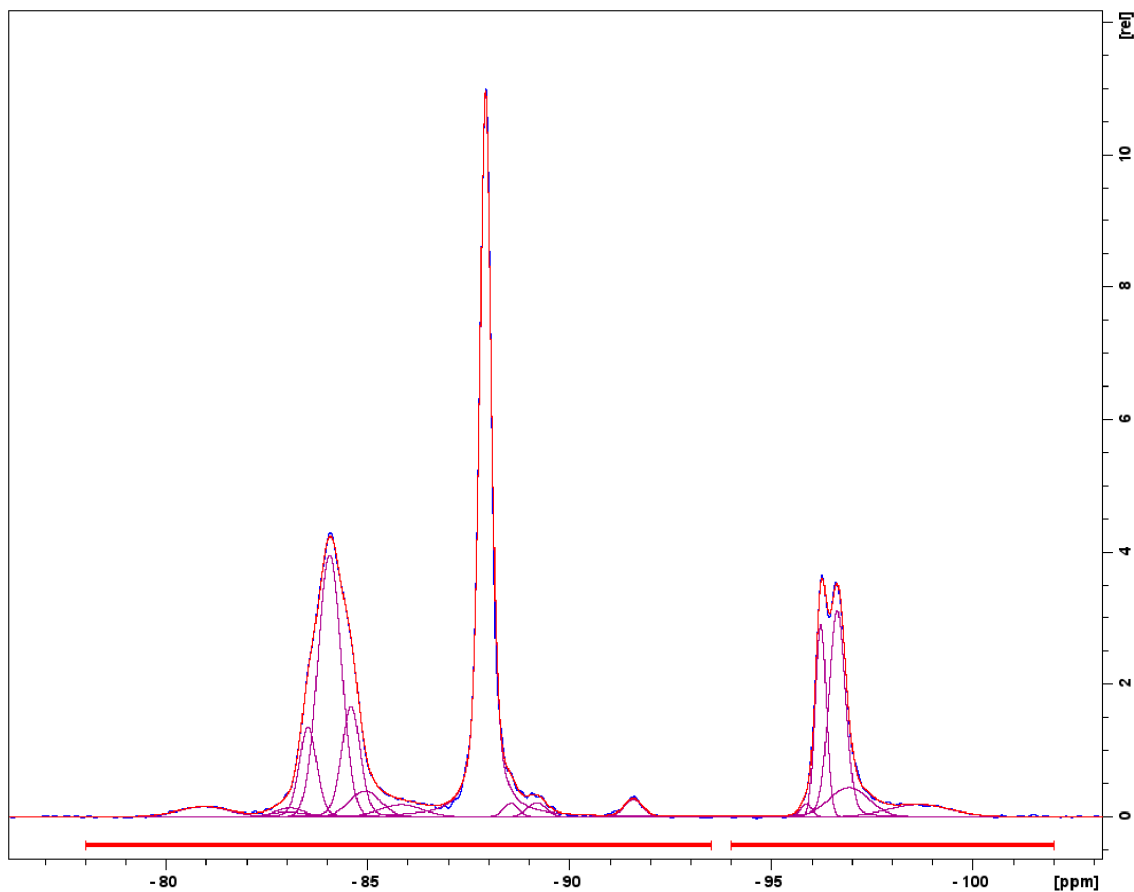
Figure 4s. The ^{1}H-^{29}Si CP MAS NMR spectrum obtained at a spinning rate of 10 kHz and contact time of 20 ms for sample 1 (same as Fig. 2b)(blue), the simulated spectrum with 17 pseudo-Voigt components (red), and the individual components (purple). The horizontal red lines delineate the frequency range of fitting. (See Table 3s for detailed parameters.)
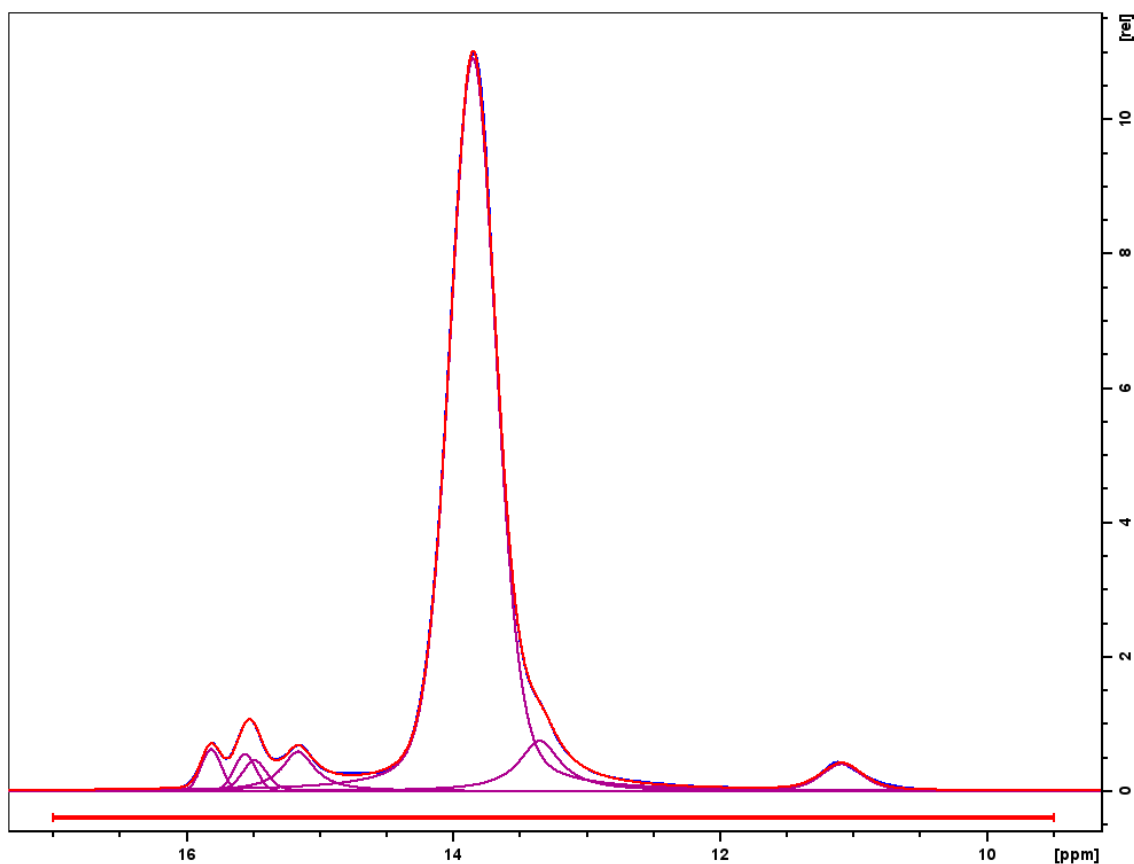
Figure 5s. ^{1}H MAS NMR spectrum obtained at a spinning rate of 24 kHz for sample 1 (same as Fig. 3a)(blue), the simulated spectrum using 7 pseudo-Voigt components (red), and the individual components (purple). The horizontal red line delineates the frequency range of fitting. (See Table 4s for detailed parameters.)
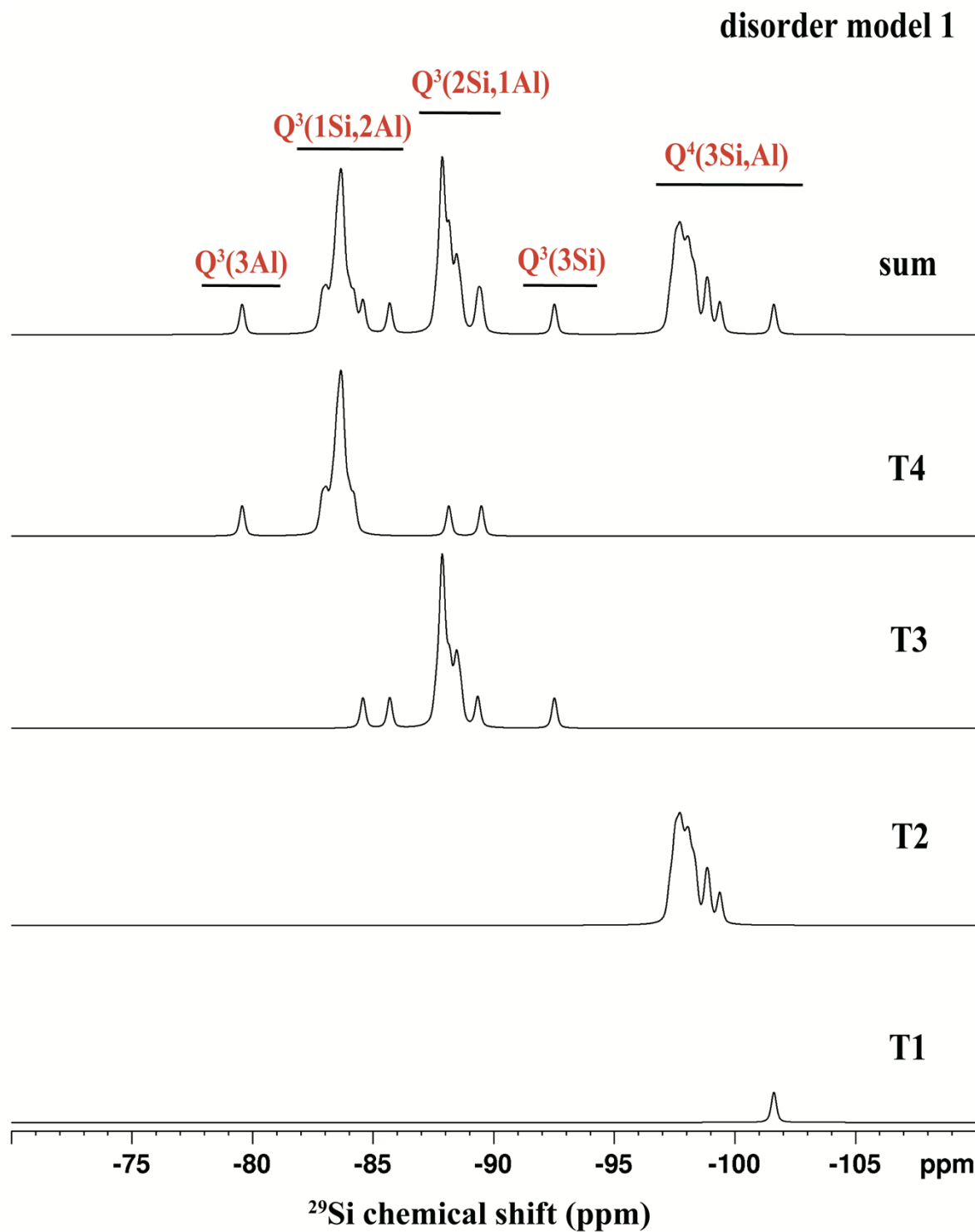
Figure 6s. Predicted ^{29}Si MAS NMR spectrum for disorder model 1 of ussingite from first-principles calculation (same as Fig. 10b), and contribution from each T site as labelled. An arbitrary Lorentzian line broadening function of 20 Hz has been applied for easy comparison.